Visual integration of vibrating images in time

Guangqing Lu,[a] Loreta Saunoriene,[b] Arvydas Gelzinis,[c] Vilma Petrauskiene,[b] and Minvydas Ragulskis[a,b,*]
[a]School of Electrical and Information Engineering of Jinan University, Zhuhai, China
[b]Kaunas University of Technology, Centre for Nonlinear Systems, Department of Mathematical Modelling, Kaunas, Lithuania
[c]Lithuanian University of Health Sciences, Department of Ophthalmology, Kaunas, Lithuania

Abstract. The ability of the human visual system to integrate a rapidly oscillating image in time is investigated in this paper. A secret image is encoded into a stochastic geometric moiré grating. The secret is leaked in the form of a pattern of time-averaged moiré fringes when the cover image is oscillated according to a predetermined law of motion. Special encoding algorithms are designed for an effective real-time implementation of the scheme on a digital computer screen. A series of experiments is performed to determine the minimum frequency of oscillations required for the interpretation of the embedded secret image. [DOI: 10.1117/1.OE.57.9.093107]

Keywords: optical illusion; time-averaging; moiré; pattern.

Paper 180898 received Jun. 22, 2018; accepted for publication Aug. 28, 2018; published online Sep. 24, 2018.

1 Introduction

Optical illusions (or visual illusions) are images perceived in a different manner compared with objective reality.[1,2] Visual view of the objects seen by the human eye is formed in our eyes and strongly depends on the brain's reaction to visual stimulus.[3,4] While in the past, visual illusions were studied mostly by psychologists, now it is the field of interest for scientists working in other fields, such as neurology, physiology, philosophy, mathematics, and computational sciences. Therefore, visual illusions are being studied from different aspects and using different tools.

Optical illusions are often classified into categories of physical and cognitive or perceptual illusions. Physical illusions comprise visual illusions that appear due to the disturbance of light between objects and the retina as well as illusions that occur due to the disturbance of neural signals. Physical illusions are the effects of excessive stimulation or interaction with stimuli of a specific type on the human eyes or brain. Such stimulation can include brightness, color, position, size, movement, etc.[3] Cognitive illusions are extremely different and appear due to the misapplied knowledge or misapplied rules.[5] Physical illusions related to movement generally include illusory motion illusions and motion-induced illusions.[6] Illusory motion (or apparent motion) is an optical illusion in which a static image appears to be moving due to the interaction of color contrasts and shape position.[7–10] Motion-induced phenomena appears due to the movement of the pattern either due to the eye or head oscillations and includes numerous problems discussed by different scientists and in different aspects. In this paper, we focus only on such visual illusions, which originate as a result of motion of a cover image.

Pritchard demonstrated the influence of eye movements on several well-known visual illusions.[11] Certain regular stationary patterns produce illusory shadows that appear to move across the pattern in normal vision. If the effect of eye movements is removed, the image on the retina is stationary and these shadows are not visible. Following these studies, Millodot[12] demonstrated the role of microfluctuations of accommodation in the viewing of the concentric ring illusion. Junge[13] gave an account of the history of explaining the moving radii illusion. This illusion appears when a set of concentric circles is subjected to a rinsing motion. In the subsequent article, Junge explained that intensity of the receptor processes depends on the time of stimulation.[14] Wade continued studying the perceptual effects generated by rotating gratings.[15] He demonstrated that rotation of a grating at a particular angular frequency results in the appearance of a band lying almost perpendicularly to the constitutive lines of the grating. Easton and Shor[16] used time exposure photography technique for the investigation of the Chevreul pendulum effect (the tendency of a small pendulum, when suspended from the hand and imaginatively concentrated on, to oscillate seemingly of its own accord). Martinetti[17] examined the effect of independently varying central, vertical, and horizontal visual angles on proportion of perceived oscillations with rotating trapezoids. Following earlier studies on rotating gratings Barbur investigated visual effects that occur while viewing rotating or rapidly approaching one-dimensional (1-D) periodic structures.[18] He presented a model explaining and predicting the effects observed during the viewing of 1-D periodic structures in terms of the temporal luminance integration in the visual system. Adelson and Movshon[19] presented their investigations on phenomenal coherence of moving gratings. They studied the conditions under which coherence does and does not occur and showed that it depends on the relative contrasts, spatial frequencies, and directions of motion of the gratings. Some years later, Anstis and Rogers[20] performed one more investigation about illusory continuous motion from oscillating positive-negative patterns. They demonstrated that small relative motion between two patterns generate two illusory effects: enhanced real movement and reversed real movement. Moreover, they revealed that dimming and brightening phases give rise to reversed apparent movement. Glünder[21] showed that a rotating sinusoidal grating is a useful sweep signal for the

*Address all correspondence to: Minvydas Ragulskis, E-mail: minvydas.ragulskis@ktu.lt

analysis of the temporal behavior of linear imaging systems. It is known that moiré patterns can produce striking movement effects and in more complex stimuli can induce vivid stereoscopic depth.[22] Spillmann[22] reviewed physical rules causing these effects and presented their relationship to psychophysics. He also proposed the use of moirés for the noninvasive examination of the human retina by aliasing. Virsu et al.[23] studied pattern perceptions caused by drifting gratings presented monocularly in the nasal and temporal visual fields at various suprathreshold contrasts. They discussed relationships between the results and retinal aliasing, cortical columns, and phase locking of neuronal oscillations. Hine et al.[24] analyzed the Ouchi illusion and its causes. Ouchi illusion is generated as a composition of two sine-wave gratings. The authors state that this illusion is potentially an important tool in understanding how higher cortical areas combine disparate motion signals. Detailed study about motion-blur illusions by Gosselin and Lamontagne was published in 1997.[25] Authors proposed a single algorithmic model explaining the still-radii illusion, the figure-of-eight illusion, the band-of-heightened-intensity illusion, and the dark-blurred-concentric-circles illusions. Until their investigation, all these visual illusions had been interpreted as isolated relatively ill-explained phenomena. In fact, Gosselin's and Lamontagne's model predicts phenomena produced by motion of any gray-shaded patterns relative to the eyes. Findings of Nishida et al.[26] provided a direct support for the existence of multiple-scale processing for first- and second-order motion in the human visual system and state that two varieties of motion are initially processed by independent pathways. In Ref. 27, it was revealed that under certain conditions, high-contrast moving figures induce adjacent illusory regions: "wakes" and "spokes." Scientists documented properties of these novel phenomena and supposed that the analyzed illusions should provide significant constraints on theories of human motion and brightness perception processes. Shorter and Patterson[28] investigated whether the stereoscopic (cyclopean) motion aftereffect (induced by adaptation to moving binocular disparity information) is dependent upon the temporal frequency or the speed of adapting motion. Nishida and Ashida[29] found that the motion aftereffect measured using a directionally ambiguous counter phase grating (flicker MAE) can be stronger when it is measured for the nonadapted eye than when measured for the adapted eye. Ehrenstein[30] analyzed basic conditions of seeing motion. He proposed that apart from the distinction between afferent (retinal) and efferent (oculomotor) mechanisms, motion percepts can result from real (object) motion as well as from various forms of apparent motion (stroboscopic or phi motion, induced motion, and autokinesis). McCourt compared the magnitudes of two suprathreshold lateral spatial-interaction effects—grating induction and contrast–contrast—with regard to their dependence upon inducing-grating spatial frequency.[31]

The main objective of this article is to present an optical illusion based on the ability of the human visual system to integrate the perceived image in time. The perception of the time-averaged image depends on the frequency of the oscillation, although mathematical relationships defining the formation of this optical effect do not depend on the frequency. An optical technique and computational setup for the detection of the minimal frequency required for the perception of secret image in the encoded cover image is also presented in this paper. This paper is organized as follows. Optical background, time-averaging operators, and optical effects are discussed in Sec. 2. Methods, the experimental, and the computational setup are discussed in Sec. 3. The results of computational experiments are discussed in Sec. 4.

2 Optical Background

Let us consider a 1-D harmonic moiré grating as a harmonic variation of a grayscale color[32]

$$F(x) = \frac{1}{2} + \frac{1}{2}\cos\left(\frac{2\pi}{\lambda}x\right), \tag{1}$$

where x is the longitudinal coordinate, λ is the pitch of the moiré grating in the state of equilibrium. Numerical value 0 of $F(x)$ represents black color, 1 is white color, all intermediate values from the interval (0,1) correspond to an appropriate grayscale level.

2.1 *Harmonic Oscillations of the Moiré Grating*

Let us consider that the harmonic moiré grating [Eq. (1)] is oscillated around the state of equilibrium according to a harmonic law of motion, and the deflection function reads $u(t) = a\,\sin t(\omega t + \varphi)$, where a is the amplitude of harmonic oscillations, ω is the frequency, and φ is the phase. If time-averaging techniques are used to register the oscillating image and the exposure time tends to infinity, then the time-averaged image $\overline{F_h}(x,a)$ (the harmonic moiré grating, harmonic oscillations) reads[33,34]

$$\overline{F_h}(x,a) = \lim_{T\to\infty}\frac{1}{T}\int_0^T\left(\frac{1}{2}+\frac{1}{2}\cos\left\{\frac{2\pi}{\lambda}[x - a\sin(\omega t+\varphi)]\right\}\right)$$
$$\mathrm{d}t = \frac{1}{2}+\frac{1}{2}\cos\left(\frac{2\pi}{\lambda}x\right)J_0\left(\frac{2\pi}{\lambda}a\right), \tag{2}$$

where J_0 is the zero order Bessel function of the first kind: $J_0(a) = \lim_{T\to\infty}\frac{1}{T}\int_0^T \exp[ia\,\sin(\omega t+\varphi)]\mathrm{d}t$;[32] $i^2 = -1$. Note that the time-averaged image does not depend neither on the frequency nor on the phase of oscillations (if only the exposure time is sufficiently long and comprises many periods of harmonic oscillations).

A schematic diagram illustrating the algorithmic approach for computational simulation of time-averaged fringes produced by harmonic oscillations of a 1-D moiré grating is presented in Fig. 1. The time-averaged image is produced by additive superposition of identical copies of the moiré grating deflected from the state of equilibrium at $(m+1)$ uniformly distributed discrete moments in time interval $[-\frac{\pi}{2\omega}, \frac{\pi}{2\omega}]$ (the higher is m, the better is the quality of the time-averaged image).

The modulating envelope function of the time-averaged image reads: $\frac{1}{2}+\frac{1}{2}J_0(\frac{2\pi}{\lambda}a)$. The time-averaged image is blurred, but this blur is nonmonotonous in respect of the amplitude a. The time-averaged image $\overline{F_h}(x,a)$ becomes uniformly gray at such amplitudes a where J_0 vanishes[33,34]

$$a = r_k\frac{\lambda}{2\pi}, \tag{3}$$

where r_k denotes the k'th root of J_0. This optical effect is shown in Figs. 2(a) and 2(b). Stationary 1-D moiré grating

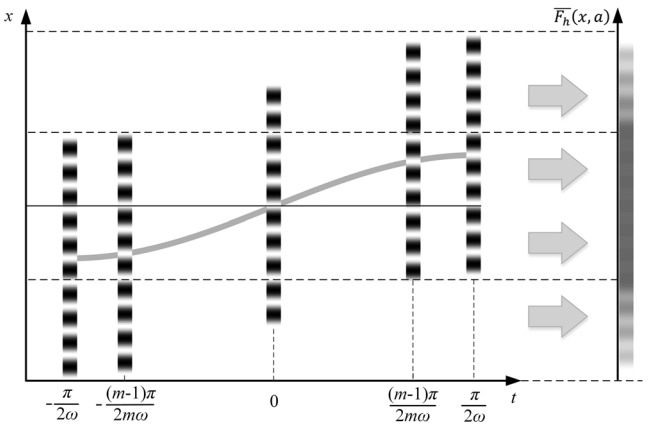

Fig. 1 Computational reconstruction of time-averaged fringes produced by harmonic oscillations of a 1-D moiré grating.

is shown at the left side of Fig. 2(a) (the amplitude $a = 0$ there). Note that the moiré grating is constructed only in a finite interval $0 \leq x \leq 10$ and the white background is assumed elsewhere. Time-averaged image of an oscillating 1-D moiré grating is visualized as a column of pixels at every discrete value of the amplitude a [Fig. 2(a)]. The graph of $J_0(\frac{2\pi}{\lambda}a)$ is shown in Fig. 2(b); dashed vertical lines indicate roots of J_0. It can be clearly seen that the centerlines of time-averaged moiré fringes do coincide with the roots of J_0 [Figs. 2(a) and 2(b)].

2.2 *Encryption of a Secret Image into the Cover Image*

Hiding the secret visual information into the background moiré image is based on the embedding of a dichotomous

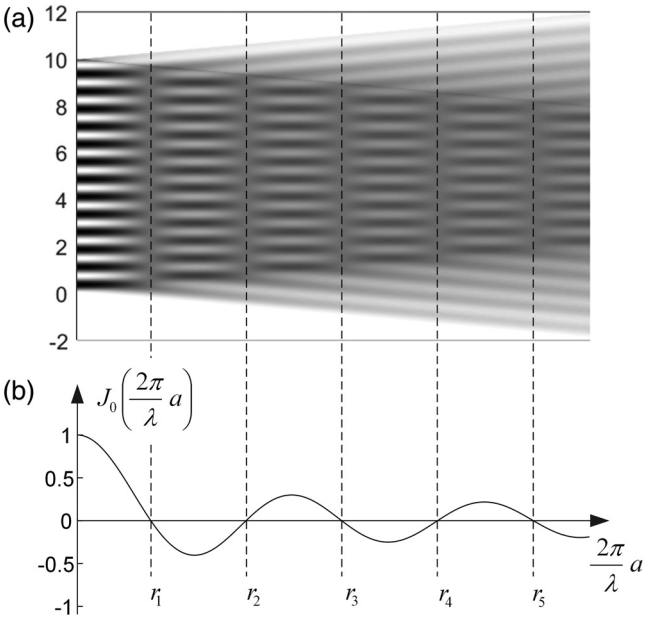

Fig. 2 Time-averaged image of an oscillating 1-D moiré grating becomes blurred. However, the optical blur is governed by a nonmonotonous envelope function. (a) Time-averaged images of a 1-D moiré grating are shown at increasing amplitudes of oscillation. (b) Dashed lines interconnect the centers of time-averaged fringes and the roots of the zero order Bessel function of the first kind.

secret image into a stationary moiré grating.[35] A straightforward embedding procedure is used: one pitch of the moiré grating λ_s is preselected to represent the secret information; another pitch λ_b is the background. A schematic 1-D example illustrating the encoding procedure is shown in Fig. 3(a). The "secret" information is placed in the middle third of the interval [0, 4.25] of the 1-D moiré grating. The upper graph in Fig. 3(a) stands for the harmonic variation of the grayscale level; the lower part shows the 1-D optical representation of that image. It can be observed that discontinuities appear at the boundaries between the secret area and the background. Such discontinuities result into sharp boundaries in the optical image and can be directly interpreted by a naked eye.

The regularization of phases at the boundaries between the secret and the background is implemented in order to avoid the discontinuities [Fig. 3(b)]. Note that the initial phase of the moiré grating at the left side of the 1-D moiré grating is left unchanged compared to Fig. 3(a). Finally, a random initial phase is assigned at the left side of the 1-D moiré grating [Fig. 3(c)]. Such encoding algorithm is used to hide a secret image in a two-dimensional (2-D) moiré grating, which is considered as an array of adjacent columns of pixels.

Figure 4 shows the encryption of a secret image into a 2-D stochastic moiré grating. The dichotomous secret image is shown in Fig. 4(a). The encoded image ($\lambda_s = 0.25$ mm, $\lambda_b = 0.3$ mm) is shown in Fig. 4(b); it is clear that the secret cannot be leaked from a static cover image by a naked eye. However, the secret is leaked as a pattern of time-averaged moiré fringes when the cover image is oscillated harmonically at $a = 0.0957$ mm and time-averaging techniques are used to register the image [Fig. 4(c)]. The secret can be perceived by a naked eye due to the contrast difference between time-averaged moiré fringes and the background area. Contrast enhancement of Fig. 4(c) represents clearer view of the hidden secret image [Fig. 4(d)].

The safety of the encoding and the quality of the decoding depend on the pitches of the moiré grating used for the secret and the background. The pitches of the moiré grating in the area occupied by the secret and in the background cannot differ significantly, otherwise the encoded secret could be interpreted by a naked eye in the static cover image. At the same time, the difference between these two pitches should be sufficient in order to ensure an appropriate contrast between time-averaged fringes and the area occupied by the background. Extensive discussion and the scheme for the determination of a near optimal pair of pitches is presented in Ref. 36.

Another important question is the information capacity of the cover image (the amount of secret visual information, which can be concealed in the cover image). These issues are thoroughly discussed in Ref. 37; the practical application of this image hiding scheme requires that the smallest component of the secret image must occupy an area not less than a single pitch of the moiré grating.

Note that moiré gratings used throughout this paper are harmonic moiré gratings. More complex moiré gratings (rectangular or even composite moiré gratings) can be used for generating different shapes in time-averaged images. Special moiré gratings can be developed for chaotic oscillations, and it is possible to construct the optimization problem where the target function is the contrast difference between the secret

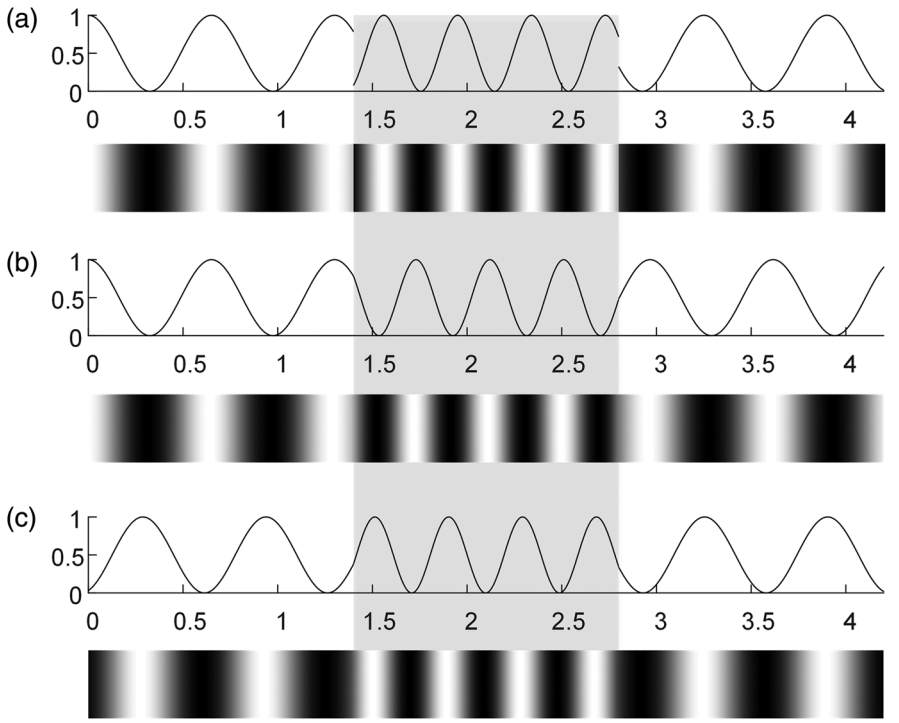

Fig. 3 A schematic illustration of the hiding scheme in a 1-D moiré grating: (a) straightforward embedding of the secret information (gray area in the graph) into the regular moiré grating; (b) secret information embedded into the regular moiré grating after phase regularization; and (c) 1-D moiré grating with a random initial phase.

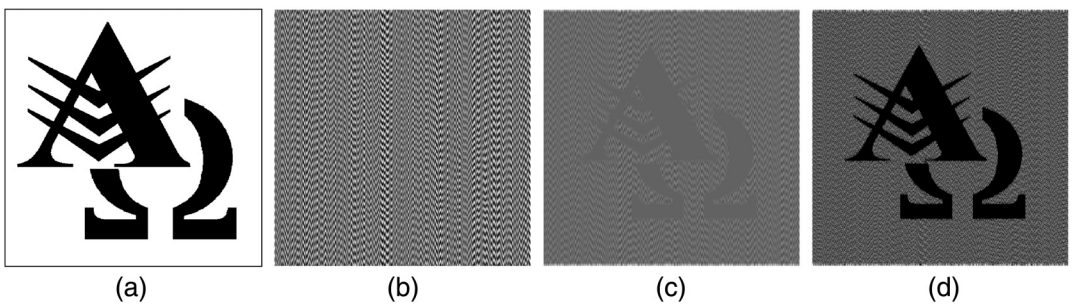

Fig. 4 Computer-based encoding and decoding of the dichotomous secret image in case of harmonic oscillations: (a) the secret image; (b) the encoded image ($\lambda_s = 0.25$ mm, $\lambda_b = 0.3$ mm); (c) time-averaged image reveals the secret at $a = 0.0957$ mm; and (d) the time-averaged image with the enhanced contrast.

and the background in the time-averaged image. It is shown in Ref. 38 that harmonic moiré gratings are not optimal for chaotic vibrations. However, virtual oscillations used in this study are periodic; therefore, moiré gratings are harmonic.

In principle, chaotic or even random oscillations could be generated on a computer screen. The rectangular waveform should be replaced by a random waveform then. The cover image can be shifted in a random number of pixels from the state of equilibrium at every time moment. However, such waveforms and chaotic (random) virtual vibrations fall out of the scope of this paper.

3 Methods

3.1 *Real-Time Implementation of the Presented Image Hiding Technique*

Optical time-averaging can be implemented using an experimental setup based on a vibrating shaker table. The encoded image can be printed by an ordinary digital printer and glued on a firm panel mounted on the head of the shaking table.[39,40] Alternatively, vibrating micro-optical electromechanical systems (MOEMS) can be used to project computer-generated holograms onto the projection plane.[41] The visual decoding (the interpretation of the pattern of time-averaged fringes) can be performed by a naked eye or by a camera with a sufficiently long exposure time. However, the exploitation of vibration generation equipment or MOEMS is inconvenient, because it requires expensive laboratory equipment. Computational real-time implementation of the presented image hiding techniques based on a virtual vibration (encoded onto moiré patterns) would open a potential for a whole range of applications.

Mathematical relationships in Eq. (3) show that the vibration frequency does not have any effect to the formation of time-averaged moiré fringes [the exposure time tends to infinity in Eq. (3)]. However, the vibration frequency does

play a primary role in visual decoding of the secret image. The human visual system is not able to recognize the hidden secret at low frequencies because eyes follow a slowly oscillating cover image. The pattern of time-averaged moiré fringes is interpreted and recognized by the human visual system only when the vibration frequency is so high that eyes stop following the rapid oscillation of the cover image. The vibration frequency can be continuously increased until a person recognizes the secret image (the vibration amplitude must be preserved constant during this experiment). This threshold (the magnitude of the vibration frequency) when the secret is visually decoded can serve as an important parameter characterizing the functionality of the human visual system.

However, there are two technical constraints related to the implementation of high-frequency oscillations of a digital image in a computer screen. The first one is the finite resolution of a digital image, and the smallest movement of the image is predetermined by the physical distance between adjacent pixels. In other words, every displacement on the computer screen is a multiplier of the size of the pixel. The second constraint is the finite refreshment rate of the digital display.

A qualitative mimicking of harmonic oscillations would require about 16 frames per period. However, the frequency of oscillations should be no less than 20 Hz in order for a naked eye to perform averaging in time (a detailed study of this frequency is the main objective of this article). It means that the implementation of harmonic oscillations on the computer screen would require a refreshment rate to be equal to 320 Hz. That is simply impossible, because the maximum refreshment rate of most ordinary monitors is 60 Hz.

3.2 *Optical Relationships Governing Oscillations According to a Rectangular Waveform*

A possible solution to these problems could be oscillations according to a rectangular waveform. Only two frames per period are required then. The deflection from the state of equilibrium reads:

$$u(t) = \begin{cases} -a \; at \; t \in \left[-\frac{\pi}{2\omega}; 0\right]; \\ a \; at \; t \in \left[0; \frac{\pi}{2\omega}\right]. \end{cases} \tag{4}$$

Then, time-averaged image of the moiré grating reads:

$$\overline{F_r}(x,a) = \lim_{T\to\infty} \frac{1}{T} \int_0^T \left(\frac{1}{2} + \frac{1}{2}\cos\left\{\frac{2\pi}{\lambda}[x - u(t)]\right\}\right) \mathrm{d}t = \frac{1}{2} + \frac{1}{2}\cos\left(\frac{2\pi}{\lambda}x\right)\cos\left(\frac{2\pi}{\lambda}a\right). \tag{5}$$

A schematic diagram illustrating the computational approach to simulation of time-averaged image produced by a 1-D moiré grating oscillating according to a rectangular waveform is shown in Fig. 5. The time-averaged image is produced by additive superposition of two identical copies of the moiré grating at the state of maximum deflections from the state of equilibrium.

The modulating envelope function now takes the following form: $\frac{1}{2} + \frac{1}{2}\cos(\frac{2\pi}{\lambda}a)$. The time-averaged image $\overline{F_r}(x,a)$ becomes uniformly gray at the roots of the cosine function $\frac{2\pi}{\lambda}a = \frac{\pi}{2}(2n+1), n = 0,1,2,3,\ldots$. This optical effect is shown in Figs. 6(a) and 6(b). Computer-based encoding and decoding of the dichotomous secret image [Fig. 4(a)] in case of the rectangular waveform oscillation are shown in Fig. 7.

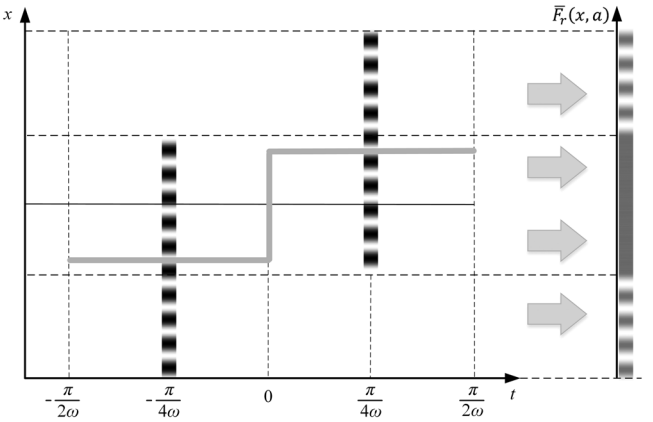

Fig. 5 Computational reconstruction of time-averaged fringes produced by a 1-D moiré grating oscillating according to a rectangular waveform.

3.3 *Protocol of the Experiment*

The main objective of the experiment is to investigate the ability of the human visual system to perform averaging in time. Two images (the arrow and the star) were encoded into a stochastic moiré cover image (Fig. 8). Adobe Flash Professional CS6 software is used to mimic the process of

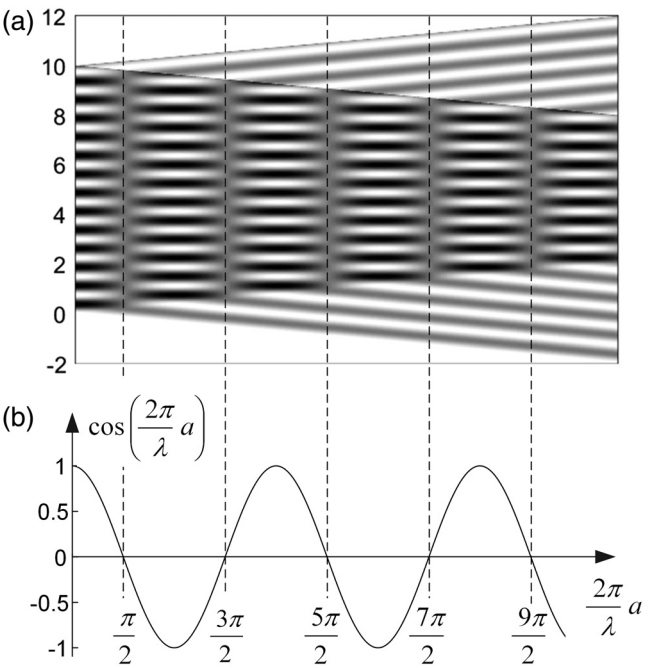

Fig. 6 (a) Time-averaged images of a 1-D moiré grating are shown at increasing amplitudes of oscillation according to the rectangular waveform. (b) Dashed lines interconnect the centers of time-averaged fringes and the roots of the cosine function.

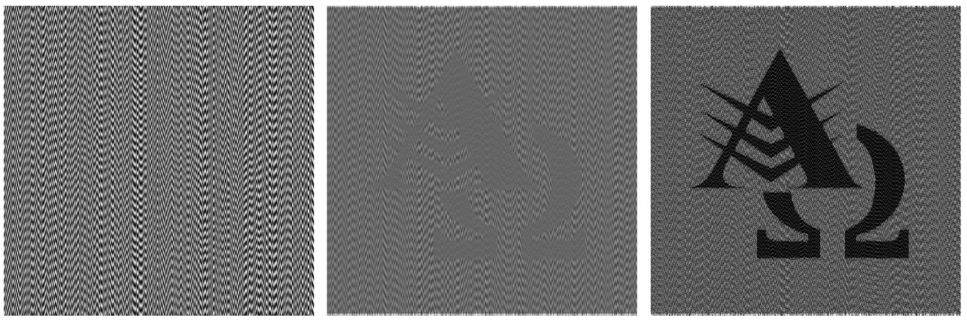

Fig. 7 Computer-based encoding and decoding of the dichotomous secret image in case of the rectangular waveform [the secret image is the same as used in Fig. 4(a)]: (a) the encoded image ($\lambda_s = 0.25$ mm, $\lambda_b = 0.3$ mm); (b) time-averaged encoded image reveals the secret at $a = 0.0625$ mm; and (c) the time-averaged image with the enhanced contrast.

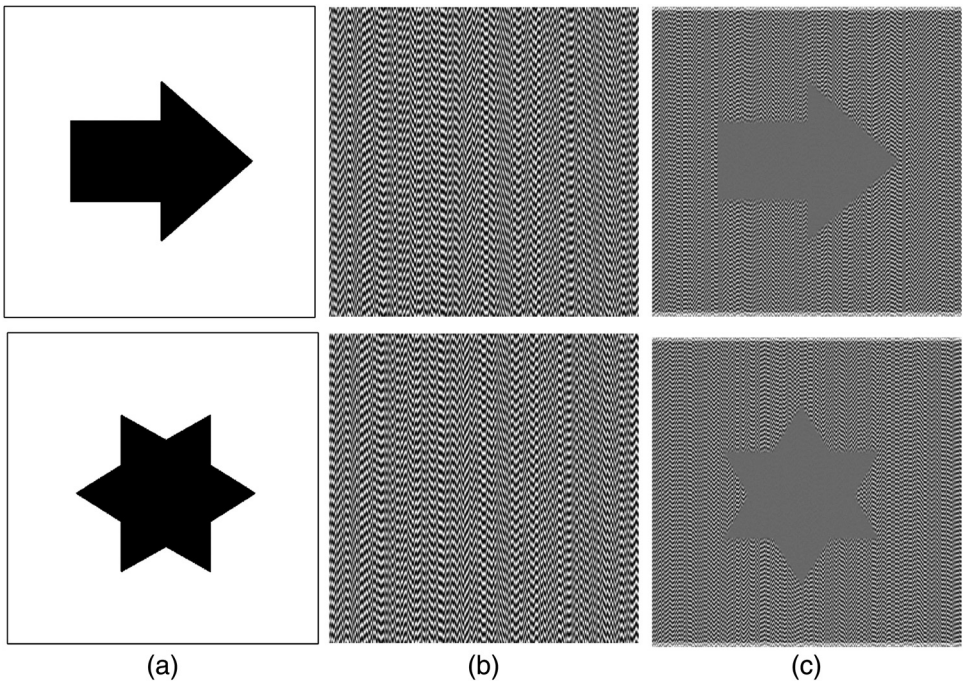

Fig. 8 Secret images used for the experiment: (a) the secret images (the arrow and the star); (b) the encoded images; and (c) the decoded images in the time-averaged mode.

oscillations according to a rectangular waveform. A person is asked to watch the computer screen and to inform when he is able to see an interpretable geometric shape. The oscillating cover image is displayed for 10 s. If the person cannot interpret the image, the frequency is increased and the process is continued until the person reports the shape of the secret image. The test is commenced at 10 Hz and the oscillation frequency is increased by 2 Hz every 10 s. The experiment is terminated either when the person tells the shape of the secret image, or the frequency reaches 50 Hz. The experiment is repeated two times with every person (with the images of the arrow and the star).

The general view of the experimental setup is shown in Fig. 9. Such a setup provides the possibility to gradually increase the oscillation frequency until the human visual system is capable of recognizing the encoded secret.

4 Results and Discussion

4.1 *Ethics Statement*

The research met all applicable standards for the ethics of experimentation. Permission to perform biomedical investigation was granted by Kaunas Regional Ethics Committee for Biomedical Investigations, No. BEC-LSMU(R)-69, 22.06.2017. Each participant provided a written consent prior to the experiment.

4.2 *Discussion*

The group of participants comprised 61 persons (15 men and 46 women). The age of participants was in the range of 18 to 30 years. None of the participants did wear spectacles or eye lenses. Each person was sitting on a chair with an adjustable

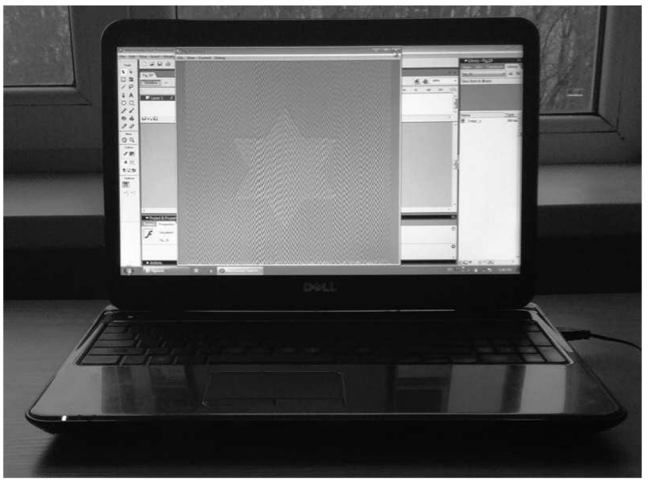

Fig. 9 The general view of the experimental setup.

height in such a position that the center of the display was in the center of the eyesight. The distance between the display and the face was 1 m. All experiments were performed in the daytime with natural ambient light; the curtains on the windows in the background of the computer screen were closed. Each person had to identify two encoded images (the arrow and the star). The minimum frequency required to perceive the secret was recorded for each person for both images. Statistical analysis shows (Fig. 10) that the lowest minimal frequency of perceiving the secret images is 16 Hz, highest 44 Hz; average minimal frequency required to recognize the arrow is equal to 27.71 Hz and the star 26.62 Hz. For men, the average minimal frequencies are: 25.54 Hz for the arrow and 25.23 Hz for the star. For women, the average minimal frequencies are 28.38 Hz for the arrow and 27.05 Hz for the star. Minimal frequencies are not normally distributed, therefore we use Wilcoxon rank sum test to check if the gender has a significant influence on the minimal frequency required to recognize the arrow and the star. As the obtained p-values of Wilcoxon rank sum test are not less than the significance level 0.05 (p-value is equal to 0.1429 for the arrow and 0.4315 for the star), we can conclude that the gender does not have a meaningful influence on the minimal frequency required to recognize the secret image.

The results of this study demonstrate that all participants were able to interpret the secret image. However, the distribution of frequencies is rather wide for both symbols (it is interesting to note that frequencies for individual persons required to identify the arrow and the star are almost identical). The objective of this paper is to show that the human visual system is capable to perform optical averaging in time. A positive answer to this question only opens a large number of additional questions. We will raise only few of many possible questions. Is there any relationship between the human fatigue and the minimal frequency required to decode the secret? Is it possible to perform the identification of some possible defects of the human visual system based on the minimal frequency?

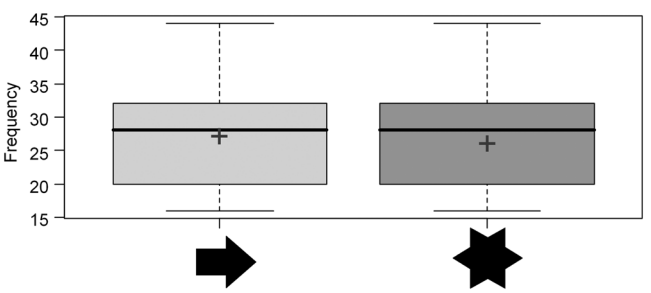

Fig. 10 The boxplot of the minimal frequencies at which the secret image is perceived by the human visual system. Gray crosses indicate the average minimal frequencies for each encoded secret image (the arrow and the star).

Note that the nonmonotonous envelope function modulating the optical blur in the time-averaged image (zero-order Bessel function of the first kind) does not depend on the frequency of oscillations [Eq. (2)]. It depends only of the amplitude of oscillations. Therefore, if we would wish to study the human perception of the modulating function, we should change not only the frequency but also the amplitude of oscillations. However, this goes beyond the scope of this paper. The amplitude of the virtual vibration is fixed to the exact value resulting into the first root of the modulating function. The only question raised in this paper is the ability of the human visual system to integrate vibrating images in time (finding the threshold frequency).

It is clear that answering to these questions requires thorough additional studies which go far beyond the objective of this paper. It is well known that the vibration of the display in a moving vehicle has a negative effect on visual performance.[42] However, the importance of these questions could be illustrated by the following entertaining example. It is easy to detect if a driver has been consuming alcohol; breath alcohol testers can give instantaneous readings. It is more difficult to check if a driver is under the influence of drugs. A blood test in a medical laboratory is usually required then. But a driver who has been driving for the last 24 h without a rest is dangerous too. A police officer could ask a suspicious driver to say what does he see in the screen of the smartphone, and if the driver cannot interpret the secret in the oscillating cover image, he could be asked to step out of the car. Of course, this could be a very far goal, but these types of investigations do remain a definite objective of future research.

As mentioned previously, effects of display vibration are studied in the field of vehicle displays.[42] However, the objective of this paper is different. We are focusing on the ability of the human visual system to integrate vibrating images in time. This aspect of visual perception goes beyond the problems associated to vehicle displays. The stationary cover image in our experimental setup is not interpretable at all, whereas images generated by vehicle displays must be interpretable both in stationary and vibrating displays.

5 Conclusions

This paper presents an image hiding technique based on the ability of the human visual system to integrate rapidly oscillating images in time. Optical relationships show that the vibration frequency does not have any influence on the formation of the time-averaged image; however, the frequency is an essential parameter for visual interpretation of the time-averaged image. This paper is mainly focused on the implementation of real-time oscillations of the cover image and

the ability of the human visual system to interpret the time-averaged image. Generation of virtual oscillations on a computer screen builds the background for experimental investigation of a special motion-induced illusion. This illusion is based on the ability of the human visual system to integrate vibrating images in time. As mentioned previously, many interesting applications of this visual effect will be considered in the future, but this paper constructs the necessary framework for further investigations.

Special algorithms are developed for the computational implementation of real-time oscillations of the cover image on the digital computer screen. Such an approach opens interesting opportunities for investigation of different aspects of visual integration in time. And though this paper is focused only on the determination of the minimal oscillation frequency required for visual interpretation of the encoded image, further aspects of visual integration remain definitive objectives of future research.

Acknowledgments

This research was supported by the Research, Development and Innovation Fund of Kaunas University of Technology (Grant No. PP32/1813). Financial support from the National Natural Science Foundation of China under Project No. 51475211 is also acknowledged.

References

1. N. J. Wade, "Op art and visual perception," *Perception* **7**, 21–46 (1978).
2. D. M. MacKay, "Interactive processes in visual perception," in *Sensory Communication*, W. A. Rosenblith, Ed., The MIT Press, London (2012).
3. R. L. Gregory, *Eye and Brain: The Psychology of Seeing*, Princeton University Press, Princeton, New Jersey (2015).
4. B. Olveczky, S. Baccus, and M. Meister, "Segregation of object and background motion in the retina," *Nature* **423**, 401–408 (2003).
5. D. Myers, "Levels of motion perception," in *Psychology in Modules*, L. Harris and M. Jenkin Eds., Worth Publishers, New York (2003).
6. S. M. Anstis, *Levels of Perception*, Springer-Verlag, New York (2003).
7. M. H. Pirenne, "Moving visual images produced by regular stationary patterns," *Nature* **181**, 362 (1958).
8. S. M. Anstis, "The perception of apparent movement," *Philos. Trans. R. Soc. Lond. B Biol. Sci.* **290**, 153–168 (1980).
9. S. M. Anstis, "Experiments on motion aftereffects," in *Computational and Psychophysical Mechanisms of Visual Coding*, L. Harris and M. Jenkin Eds., Cambridge University Press, Cambridge, New York (1997).
10. G. Mather, F. Verstraten, and S. Anstis, *The Motion After Effect: A Modern Perspective*, The MIT Press, Cambridge, Massachusetts (1998).
11. R. M. Pritchard, "Visual illusions viewed as stabilized retinal images," *Q. J. Exp. Psychol. A* **10**, 77–81 (1958).
12. M. Millodot, "Influence of accommodation on the viewing of an optical illusion," *Q. J. Exp. Psychol. A* **20**, 329–335 (1968).
13. K. Junge, "Final note on the moving radii illusion," *Scand. J. Psychol.* **4**, 134 (1963).
14. K. Junge, "The moving radii illusion," *Scand. J. Psychol.* **4**, 14–16 (1963).
15. N. J. Wade, "Some perceptual effects generated by rotating gratings," *Perception* **3**, 169–184 (1974).
16. R. D. Easton and R. E. Shor, "Information processing analysis of the Chevreul pendulum illusion," *J. Exp. Psychol. Appl.* **1**, 231–236 (1975).
17. R. F. Martinetti, "The effect of visual angle orientation on perceived oscillatory motion," *J. Gen. Psychol.* **94**, 59–64 (1976).
18. J. L. Barbur, "Quantitative studies of some dynamic visual effects," *Perception* **9**, 303–316 (1980).
19. E. H. Adelson and J. A. Movshon, "Phenomenal coherence of moving visual patterns," *Nature* **300**, 523–525 (1982).
20. S. M. Anstis and B. J. Rogers, "Illusory continuous motion from oscillating positivenegative patterns: implications for motion perception," *Perception* **15**, 627–640 (1986).
21. H. Glünder, "Rotating gratings reveal the temporal transfer function of the observing," *J. Mod. Opt.* **34**, 1365–1374 (1987).
22. L. Spillmann, "The perception of movement and depth in moiré patterns," *Perception* **22**, 287–308 (1993).
23. V. Virsu, J. Rovamo, and P. Laurinen, "Illusory perception of gratings stimulating a small number of neurones," *Vision Res.* **34**, 3253–3263 (1994).
24. T. Hine, M. Cook, and G. T. Rogers, "The Ouchi illusion: an anomaly in the perception of rigid motion for limited spatial frequencies and angles," *Percept. Psychophys.* **59**, 448–455 (1997).
25. F. Gosselin and C. Lamontagne, "Motion-blur illusions," *Perception* **26**, 847–855 (1997).
26. S. Nishida, T. Ledgeway, and M. Edwards, "Dual multiple-scale processing for motion in the human visual system," *Vision Res.* **37**, 2685–2698 (1997).
27. A. O. Holcombe et al., "Wakes and spokes: new motion-induced brightness illusions," *Perception* **28**, 1231–1242 (1999).
28. S. Shorter and R. Patterson, "The stereoscopic (cyclopean) motion aftereffect is dependent upon the temporal frequency of adapting motion," *Vision Res.* **41**, 1809–1816 (2001).
29. S. Nishida and H. Ashida, "A motion aftereffect seen more strongly by the non-adapted eye: evidence of multistage adaptation in visual motion processing," *Vision Res.* **41**, 561–570 (2001).
30. W. H. Ehrenstein, "Basics of seeing motion," *Arq. Bras. Oftalmol.* **66**, 44–52 (2003).
31. M. E. McCourt, "Comparing the spatial-frequency response of first-order and second-order lateral visual interactions: grating induction and contrast–contrast," *Perception* **34**, 501–510 (2005).
32. A. S. Kobayashi, *Handbook on Experimental Mechanics*, 2nd ed., SEM, Bethel, Connecticut (1993).
33. C. Y. Liang et al., "Time-averaged moiré method for in-plane vibration analysis," *J. Sound Vib.* **62**, 267–275 (1979).
34. M. Ragulskis and Z. Navickas, "Time-average geometric moiré–back to the basics," *Exp. Mech.* **49**, 439–450 (2009).
35. M. Ragulskis and A. Aleksa, "Image hiding based on time-averaging Moiré," *Opt. Commun.* **282**, 2752–2759 (2009).
36. L. Saunoriene, S. Aleksiene, and J. Ragulskiene, "Near-optimal pitch of a moiré grating for image hiding applications in dynamic visual cryptography," *Vibroeng. Procedia* **13**, 266–271 (2017).
37. R. Palivonaite et al., "Image hiding in time-averaged deformable moiré gratings," *J. Opt.* **16**(2), 025401 (2014).
38. M. Ragulskis, M. Sanjuan, and L. Saunoriene, "Applicability of time average moiré techniques for chaotic oscillations," *Phys. Rev. E* **76**, 036208 (2007).
39. V. Petrauskiene et al., "Dynamic visual cryptography for optical control of vibration generation equipment," *Opt. Lasers Eng.* **50**(6), 869–876 (2012).
40. V. Petrauskiene and L. Saunoriene, "Application of dynamic visual cryptography for optical control of chaotic oscillations," *Vibroeng. Procedia* **15**, 81–87 (2017).
41. P. Palevicius and M. Ragulskis, "Image communication scheme based on dynamic visual cryptography and computer generated holography," *Opt. Commun.* **335**, 161–167 (2015).
42. M. J. Moseley and M. J. Greffin, "Effects of display vibration and whole-body vibration on visual performance," *Ergonomics* **29**(8), 977–983 (1986).

Guangqing Lu received his first PhD in mechanical engineering at Xi'an Jiaotong University, China, in 1996, and his second PhD in engineering science and mechanics from the University of Alabama, USA, in 2004. He was working as a fellowship researcher at LG Electronics, Inc., in Seoul, Korea, from 1997 to 1998 and as a post-doctoral researcher at the Department of Mechanical Engineering, the University of Alabama, from 1998 to 2001. Currently, he has beeen an associate professor at the School of Electric and Information Engineering, Jinan University, China, since 2005.

Loreta Saunoriene received her PhD from Kaunas University of Technology, Lithuania, in 2007. She has been an associate professor at the Department of Mathematical Modelling in Kaunas University of Technology, Lithuania, since 2005, and a member of the Center for Nonlinear Systems, Kaunas University of Technology.

Arvydas Gelzinis received his MD degee in ophthalmology from Kaunas Medicine University in 2003 and his PhD from Lithuanian University of Health Sciences in 2012. Currently he has been a lecturer at Lithuanian University of Health Sciences, ophthalmologist and chief of the Pediatric Ophthalmology Department at the Hospital of Lithuanian University of Health Sciences Kauno Klinikos since 2012. His fields of interest are pediatric ophthalmology, disorders of binocular vision, and clinical electrophysiology of vision.

Vilma Petrauskiene received her PhD from Kaunas University of Technology, Lithuania, in 2015. She has been a lecturer at the Department of Mathematical Modelling in Kaunas University of Technology, Lithuania, since 2009, and a member of the Center for Nonlinear Systems (Kaunas University of Technology).

Minvydas Ragulskis received his PhD from Kaunas University of Technology, Lithuania, in 1992. He has been a full professor at the Department of Mathematical Modelling (Kaunas University of Technology) since 2002 and has been the head of the Center for Nonlinear Systems (Kaunas University of Technology) since 2016. Also, he has been a chair and honorary professor at the School of Electric and Information Engineering, Jinan University, China, since 2017.